

Mapping of composition-rheology relationships in polymer composite-type precursors

Caitlin A. Grover¹ | Cindy Bonilla Bernal¹ | Irmak Sargin² |
 Scott P. Beckman¹ | B. Arda Gozen¹ 

¹School of Mechanical and Materials Engineering, Washington State University, Pullman, Washington, USA

²Department of Metallurgical and Materials Engineering, Middle East Technical University, Ankara, Turkey

Correspondence

B. Arda Gozen, School of Mechanical and Materials Engineering, Washington State University, Pullman, WA, USA.
 Email: arda.gozen@wsu.edu

Funding information

U.S. Department of Defense,
 Grant/Award Number: W911NF-23-2-0087; National Science Foundation,
 Grant/Award Number: CMMI-1846758

Abstract

Considering their simplicity, processibility, and tunable rheological properties, polymer composite-type precursors hold exceptional promise in the processing of polymers, ceramics, metals, and their composites. This large variety of precursors used in many different applications cover a large compositional space with dramatically varying rheological properties. Understanding how precursor composition influences their rheological properties is a key need towards streamlining the design and implementation of these precursors. With regard to this design advancement, this study elucidates the composition-rheology relationships of graphene-poly(ethylene) oxide (PEO) composite inks as a sample polymer composite-type precursor. To this end, shear and extensional rheology of numerous compositions were studied across a wide compositional space, which varied graphene concentration, total solid concentration, and binder molecular weight. These studies showed that composition greatly affected various rheological parameters, such as the overall presence of yielding behavior. Specifically, this study illustrated the influence of (i) binder structure, (ii) total solid loading, and (iii) binder-filler interactions on ink rheology. Extensional rheology was studied to examine how relaxation behaviors were dependent on composition and explicate how relaxation behaviors coincide with responses to shear forces. In tandem, our results illuminate significant composition-rheology relationships in polymer composite-type precursors.

Highlights

- Rheology of polyethylene oxide-graphene composite precursors were studied.
- Shear and extensional rheology, and their correlations were investigated.
- Composition-binder molecular weight-yielding relationships were elucidated.
- Extensional relaxation regimes were identified with respect to composition.
- Results can be used to determine compositional ranges for different processes.

KEY WORDS

extensional rheology, graphene, poly(ethylene) oxide, processing, shear rheology, yield stress

1 | INTRODUCTION

Material precursors used in the processing of polymers and their composites as well as metals, ceramics, and their composites (through the powder processing route) share a common compositional profile consisting of a non-crosslinked polymer matrix in a melt or solution form and solid particulates. The examples range from various gels, inks, and slurries to pastes, castables, molding compounds, and clays. These material-diverse precursors are simple to work with, can be directly shaped, and their flow properties can be tuned according to specific processing methods, including electrospinning, fiber pulling, injection and extrusion molding, casting, and three-dimensional (3D) printing.^{1,2} A diverse range of materials means these precursors can be used in many applications, depending on the target material the precursor should yield. For example, polymer composites can be manufactured using these precursors, and they can be found in applications such as biosensing, tissue engineering, and drug delivery.³ Ceramics and their composites could also be manufactured using these precursors, and they can be found in fields ranging from biomedical to ultrahigh temperature applications.^{4,5} Depending on the material type, processing of these precursors follows different routes. In the case of polymers and polymer composites, the final product is obtained following the solidification of the polymer matrix. For metals and ceramics, polymer solidification leads to a green body. The green body is then thermally processed to burn off the polymer matrix to obtain a brown body which is then sintered to obtain the final product.⁶ Considering the broad application of these materials, there is pervasive need to elucidate their composition-processing-property relationships in a generalizable way.

Flow and deformation of these materials is central to their processing as these factors directly influence key processing methods and parameters as well as properties of the final products including microstructure, density, and functional properties. Regarding the processing methods, different material domains and processing approaches require precursors with different flow behaviors.^{7,8} For instance, screen printing of polymers and their composites rely on the ease of flow and spreading of low viscosity inks, whereas high viscosity, shapable clays and pastes are used in various ceramics processing methods. Regarding the final properties of manufactured parts, it has been shown that the shear deformations experienced by the

precursors during processing dictate the distribution and orientation of fibrous fillers in various composites,^{9–12} and thus the final functional properties. This diversity of required precursor flow behavior calls for an extensive research focus on material rheology. Material composition is the primary factor influencing rheology with the relevant factors including solid loading, polymer to particle ratio and polymer molecular weight. These precursors cover a broad compositional spectrum, ranging from highly loaded pastes or clays for ceramics and metals to viscous melts or low viscosity inks with lower solid concentration, primarily used for polymer processing. Accordingly, they exhibit a broad range of rheological behavior. Considering a general set of constituents for these materials, the relevant research found in the literature regarding their composition-rheology relationships lies in the polymer composites domain.

There have been many rheological studies on polymer composites with a wide range of fillers, including organoclays,^{13–15} fumed silica,^{13,16} and carbon-based materials such as carbon black, carbon nanotubes, and graphene.^{17–19} The concentration of these particles as well as polymer structure greatly influence the rheology, flow-induced microstructure, and therefore final properties of a polymer composite. As such, a very broad spectrum of rheological properties can be observed through various compositional parameters. Most prominently, a characteristic shift from liquid- to solid-like behavior is observed with increasing filler content. At a certain filler concentration, referred to as the percolation threshold, a filler network forms, having significant implications on the material rheology. Under shear forces, the network undergoes formation and destruction, leading to a solid-to-liquid transition, thus the emergence of the yield stress.²⁰ This solid- to liquid-like behavior is critical to certain processing methods, such as extrusion-based 3D printing and, as such, has been studied in detail. Furthermore, it is attributed to the appearance of the Payne effect,²¹ which is characterized by a sharp decrease in the storage modulus preceded by a plateau, at low strain rates. Lower filler concentrations generally lead to a lack of yield stress and lower overall precursor viscosity. In that domain, there are numerous studies focusing on graphene-based polymer composites, highlighting the fact that low concentrations of graphene can lead to significant performance enhancements.^{22,23} The low viscosity and lack of solid-liquid transition in these precursors enable their easy flow and spreading, which are critical

for several processing methods including but not limited to injection molding and vat photopolymerization-based additive manufacturing.

While filler loading plays a substantial role in material rheology, the influence of polymer structure cannot be overlooked. For instance, the interactions between the polymer chains of the binders has been shown to lead to emergence yield stress.^{17,18} It has also been shown that when binder-filler interactions within a polymer composite occur through the adsorption on the polymer surface, microstructural evolution of the composite under flow is governed by the polymer chains adjacent to the adsorbed surfaces, rather than the adsorbed chains themselves.²⁴ Additionally, polymer molecular weight directly affects matrix viscosity, which is an important parameter for processing and particle distribution.²⁵ Given the limited number of studies on this topic, polymer structure-composite rheology relationships remain widely unexplored.

Finally, most studies on polymer composite rheology focus on the material systems where the binder in the precursor solidifies to generate a green or final part without mass loss.²⁶ It is worth noting that polymer composites can also be processed in solution form, where a solvent is used to tune precursor rheology. These types of precursors are generally referred to as inks. For most applications of these systems, such as screen printing and extrusion-based additive manufacturing, the solvent evaporates during processing to leave behind the solid constituents of the precursor, inducing a net mass loss. This processing method adds an additional compositional parameter as the total solid concentration needs to be taken into consideration.^{21–24}

As outlined above, composition-rheology relationships for polymer composite-type precursors have been studied within the context of individual compositional parameters, particularly filler concentration, with sparse focus on polymer structure and total solid concentration. As such, there is a need for a holistic study capturing how each of these different compositional parameters affect precursor rheology towards generalizable precursor design guidelines for various applications. To address these needs, we present a comprehensive study on the rheology of these precursors in a broad compositional spectrum in this article. To this end, we characterized the precursor behavior under shear and extensional flow to determine how precursor rheology varies with composition. Focusing on a precursor composition consisting of a poly(ethylene) oxide (PEO) binder and graphene platelet fillers in an aqueous solution, we varied total solid concentration, binder-filler ratio and the molecular weight of the PEO binder. On the shear rheology, we particularly investigated the compositional parameter ranges within which the yield pseudoplastic behavior is observed,

dividing the compositional space into two regions depending on the emergence of this behavior. We then separately analyzed the shear thinning nature of materials in these two regions through the fitting of rate-dependent shear stress models to the experimental data and study how various quantifiable model parameters vary as a function of composition. Similarly, for extensional rheology, experimental material relaxation profiles were fitted with well-known models. Probabilities of various material compositions conforming to these different model behaviors were analyzed. We finally discuss the connections between the shear and extensional rheology of these materials and the practical implications of the findings regarding processing. The following sections introduce the materials as well as experimental and analytical methods, followed by results, discussions, and relevant conclusions.

2 | EXPERIMENTAL PROCEDURE

2.1 | Polymer composite ink preparation

The inks studied in this article were aqueous solutions of PEO (Sigma Aldrich) with two different molecular weights: 100,000 Da (referred to as low molecular weight (LMW)) and 5,000,000 Da (referred to as high molecular weight (HMW)) and graphene nanopowder (Graphene Supermarket, Grade AO-4, 60 nm). The materials that will be referred to going forward as “HMW inks” included a binder with a 1.5:100 mixture of HMW PEO and LMW PEO, respectively. A second type of ink with a binder of only LMW PEO was also studied, and they will be referred to as “LMW inks” going forward.

To prepare inks within a large compositional range at a high throughput, “base inks” of specific compositions were prepared then combined with either other base inks or minute amounts of additional solid to create other compositions. A high-speed mixer (Cole-Parmer OS-200D-C-SYS Compact Digital Mixer) was used to mechanically mix base inks. Mixing began at 250 rpm and slowed to between 100 and 150 rpm as solids were added. LMW PEO was added first to ensure agglomeration of the graphene particles did not occur. Graphene was added second, and lastly, HMW PEO was added if a HMW ink was being prepared. When preparing a LMW ink, only the first two constituents were used. Slow and controlled hand mixing was used when combining multiple base inks or mixing in additional solids. Finished inks were stored on tube rollers for up to 48 h until characterized. All compositions are in wt%.

A particular naming convention capturing three compositional factors was used: relative graphene concentration (as in, the percent graphene in the total solid

concentration), the binder molecular weight, and the total solid concentration. For example, 80G-1.5H-30S is a HMW ink, indicated by “1.5H,” with 80% relative graphene (or, 24% total graphene), and a total solid concentration of 30%. LMW inks are named in the same way, with the distinction of “OH” rather than 1.5H. The complete list of inks that were tested are provided in Supporting information Tables S1 and S1. A total of 67 HMW inks and 61 LMW inks were prepared.

2.2 | Rheological characterization of the inks

2.2.1 | Shear rheology characterization

Shear rheology experiments were performed on a strain-controlled rotational rheometer (TA Instruments, ARES G2) using parallel plate geometry having a diameter of 25 mm with custom-machined serrated plates to minimize the effects of wall slip. A gap size of 1 mm was used for all experiments. All inks were pre-sheared at a rate of 0.001 s^{-1} for 600 s. Amplitude sweeps were carried out from 0.1% to 1000% strain at 1.0 rad/s to determine the presence of yielding behavior. Flow sweep experiments had two distinct steps. The first was from a strain rate of 0.0005 to 0.005 s^{-1} , with a set equilibration time of 600 s and an averaging time of 10 s. The second step tested strain rates from 0.005 to 0.05 s^{-1} and utilized steady state sensing with an averaging time of 10 s. The rheometer detected steady-state by sensing how the torque changed over time. Steady state was achieved if the torque values measured by the instrument were within 0.2% of one another for 10 s. However, if no steady state was achieved, there was a maximum equilibration time of 600 s. One sample of each composition was tested, but if an anomaly was seen, then the test was repeated to determine if it was real.

2.2.2 | Extensional rheology

Extensional rheology of the inks was characterized through the capillary breakup²⁷ method, particularly focusing on the relaxation phase of the experiment. These experiments were performed on the same ARES G2 rheometer under the axial mode, instrumented with a camera, and used parallel plate geometry with standard flat plates. Here, 0.1 mL of ink is sandwiched between two plates and the top plate is moved at an exponentially increasing speed to impose a constant extensional Hencky strain rate of 1 s^{-1} on the ink and create a vertical liquid bridge.²⁸ Videos of the filament thinning following the

plate movement were then recorded and can be found in the supporting videos. The maximum gap change between the plates during the deformation phase varied from 5 to 12 mm, depending on the behavior of the ink. Tests for all inks began with a 12 mm gap change; however, if the ink filament between the plates disconnected prior to the end of the plate motion, the gap change was lowered until the ink survived the experiment and data could be collected. Once the gap change was determined, all experiments were repeated 5 times. Recorded videos were then analyzed using the Image Processing Toolbox in MATLAB to quantify the diameter change over time.

2.3 | Rheological data processing

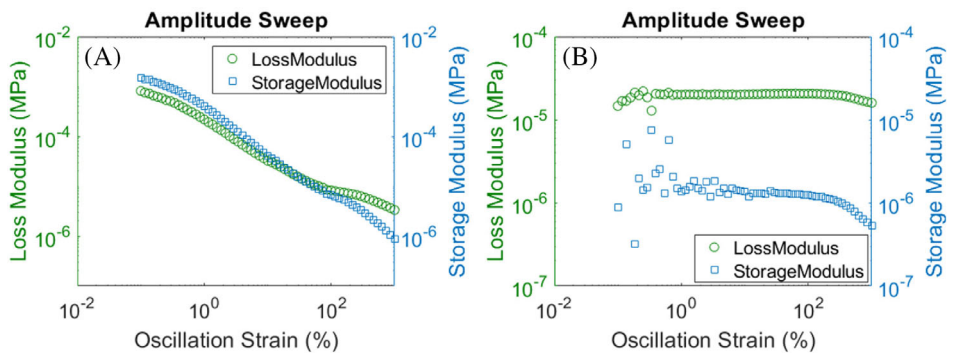
The rheological data analysis aims to understand the relationships between the ink composition and the emergence of various rheological behaviors. A particular point of interest is the classification of ink compositions with respect to the presence of yield pseudoplastic behavior, that is of importance for various processing methods including additive manufacturing. This is achieved through qualitatively examining and using a regression approach to identify the best rheological model fits to shear and extensional rheology data and extracting the quantitative model parameters associated with the best fits. The relationships between the ink composition and those quantitative variables are also studied.

2.3.1 | Shear rheology data processing

The shear rheology analysis starts by the examination of the low-strain, linear viscoelastic range of amplitude sweep data to identify the presence of the yielding behavior. In that, we quantify the $\tan(\delta)$ variable for these tests, which is defined as the ratio between the loss and storage moduli measured at this strain range. If the storage modulus was higher than the loss modulus, namely $\tan(\delta) < 1$, the particular ink was classified as a yielding material. Compositions for which $\tan(\delta) > 1$ in the linear viscoelastic range were classified as non-yielding. Example amplitude sweep data corresponding to sample yielding and non-yielding ink compositions are shown in Figure 1. A non-steady-state response at low oscillation strains was observed for all non-yielding inks.

Next, the flow sweep data is processed. In that, the stress versus strain rate data was interpolated in the strain rate domain to obtain 100 data points and fitted with material models depending on the yielding and non-yielding classification. Subsequently, materials that were deemed as yielding, the interpolated flow sweep

FIGURE 1 Examples of (A) yielding and (B) non-yielding amplitude sweeps.



data was fit to the Herschel–Bulkley–Papanastasiou (HBP) model^{29,30} as shown in Equation (1).

$$\tau = \tau_y * (1 - e^{-m\dot{\gamma}}) + k\dot{\gamma}^n. \quad (1)$$

If a given ink composition was determined to be non-yielding, the associated flow sweep data was fit to the Carreau–Yasuda³¹ and power law models:

$$\tau = \dot{\gamma} \left[\eta_\infty + (\eta_0 - \eta_\infty) (1 + (\lambda\dot{\gamma})^a)^{(n-1)/a} \right], \quad (2)$$

$$\tau = \eta x^n. \quad (3)$$

The description of each individual parameter in these models can be found in supporting information Table S3.

2.3.2 | Extensional rheology data processing

The filament diameter versus time data was fit to four models: Elastic fluid (modes 1–3), power law, Bingham plastic, and yielding, all of which are shown below.³²

$$\begin{aligned} \text{Elastic fluid: } & \frac{R(t)}{R(0)} = \sum_{n=1}^N (A_n R(0))^{1/3} \exp(-t/3\lambda_n) \text{ for } N \\ & = 1, 2, \text{ or } 3, \end{aligned} \quad (4)$$

$$\text{Power law: } \frac{R(t)}{R(0)} = a * (t_c - t)^n \text{ for } 0 < n \leq 1, \quad (5)$$

$$\text{Bingham plastic: } \frac{R(t)}{R(0)} = \left(\frac{a}{R_0} \right) [1 - \exp(b(t - t_c))], \quad (6)$$

$$\text{Yielding: } \frac{R(t)}{R(0)} = C. \quad (7)$$

As shown in Equation (7), yielding materials exhibit a constant radius and do not show any thinning during the

relaxation phase in extension. Thus, the only extractable information is that the material has a yield stress. The best fit model for given experiment was quantified using the Akaike Information Criterion (AIC), with the lowest score indicating the best balance between the complexity of the model and the goodness of fit.

$$AIC = \ln(s_z^2) + \frac{2p}{n}, \quad (8)$$

s_z^2 is the residual sum squared, p is the number of free parameters in a particular model, and n is the number of data points in each experiment. The standard AIC difference of at least 2 was used to select the best model.³³

During capillary breakup rheometry, considerable variations in ink behavior was observed across the different trials, particularly in compositions that fell within a “transition region” between different behaviors within the compositional space, which will be more thoroughly defined in subsequent sections. To objectively identify the material behavior at different compositions, the probability of a particular composition exhibiting a specific behavior was calculated. To this end, all AIC values for each trial were recorded and offset by subtracting the highest AIC from all other AIC values, such that they all had the same sign:

$$AIC_{model,i}^* = AIC_{model,i} - \max(AIC_{model,i}), \quad (9)$$

where i denotes the trial number between 1 and 5. The offset AIC values were normalized across each trial by dividing them by the lowest value as follows:

$$\overline{AIC}_{model,i} = AIC_{model,i}^* / \min(AIC_{model,i}^*). \quad (10)$$

After the normalized AIC values are calculated for each experiment, the average AIC of each model was calculated. Specifically for elastic fluid, a second average covering all three modes was taken to consolidate the three modes into one probability. The probability of a

particular composition conforming to a particular model can then be calculated as

$$P(\text{model}) = \text{mean}_i(\overline{\text{AIC}}_{\text{model},i}) \sum_{\text{model}} \text{mean}(\overline{\text{AIC}}_{\text{model},i}). \quad (11)$$

3 | RESULTS

3.1 | Shear rheology

Phase maps parameterizing rheology were created for each binder molecular weight. The way the mapped parameters were found is visually described in Supporting information Figure S1.

3.1.1 | Composition dependence of yielding behavior

Figure 2A,B shows the non-yielding (yellow) and yielding (green) regions, as well as a transitional band between the two (light green) for both HMW and LMW inks. The isoline for $\tan(\delta) = 1$ is shown in red, and the isolines for $\tan(\delta) = 0.8$ and 1.2 are shown in black. Based on the $\tan(\delta)$ conditions discussed in Section 2.3.1, we postulate that the region between the black lines is where the transition between the two classifications should lie, with the red line indicating our interpolated discrete transition line. In these figures, the dashed curves correspond to the constant absolute graphene weight concentrations.

When the transitional bands for inks with two different binder molecular weights are examined, the yielding-non-yielding transition happens to be at a fixed relative graphene concentration independent of the total solid concentration when at low total solid concentrations (10–30 wt% for HMW, 10–50 wt% for LMW) in both cases. One could accordingly conclude that the yielding behavior is driven by some form of interaction between the filler and the binder phases, rather than the concentration of one. This indicates that the yielding nature in the lower solid concentration range is not a sole function of filler percolation thresholds. Further analyses of binder-filler interactions leading to the observed behavior is outside the scope of this work. Additionally, the required amount of graphene to induce yielding is higher for HMW inks (~50 rel%) than LMW inks (~40 rel%) at the lower total solids range. The difference in graphene requirement could possibly be explained by the particle reinforcement structure, or the “house of cards” effect, and the probability of formation of such a structure in different inks. It has been shown that the house of cards effect is one of the primary sources of yield-pseudoplastic

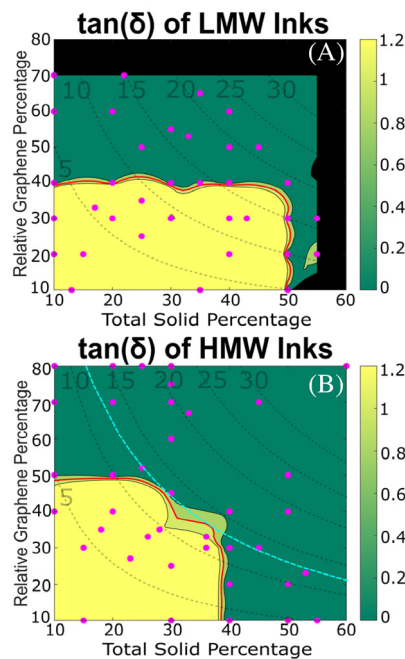


FIGURE 2 The $\tan(\delta)$ maps of (A) LMW and (B) HMW inks. The maps depict the yielding regions in green and the non-yielding regions in yellow. The two regions are separated by the transitional band shown in light green and the discrete transition line at which $\tan(\delta) = 1$, shown in red. Absolute graphene concentrations are depicted by the dotted lines. The blue dotted line, at 12 wt% absolute graphene, shows an approximate concentration controlling yielding behavior. The data outside of the pink points is interpolated for visualization purposes.

behavior, and graphene particles dispersed throughout the inks should form a similar network under Van der Waals attraction, as long as they are not impeded by the presence of the binder polymer chains.²⁰ For binders with a higher HMW polymer content, a higher amount of chain entanglement is expected, which in turn statistically reduces the probability of particle network formation thus requiring a larger overall graphene content for the networks to be formed. It should be noted that chain entanglement itself may lead to emergence of yield pseudoplastic behavior in polymers, such as in polymer gels³⁴, however, at solid concentrations as low as 10 wt%, there may not be enough polymer present in the ink to create this effect due to chain entanglement alone.

The yielding boundary for the HMW inks in the 20%–40 wt% total solid concentration range seems to fall between the 10 and 15 wt% absolute graphene concentration isolines, at approximately 12 wt%, which is shown in blue. This may indicate that in this range the absolute graphene concentration is the driving factor for the emergence of the yielding behavior, which is likely due to the increase in the total binder concentration that comes

with an increase in total solid concentration. The isoline at 12 wt% portrays an absolute graphene driven percolation threshold within a concentration range of 5–6 vol% absolute graphene across the tested space. That concentration is comparable to previous studies on other composites loaded with graphitic nanoplatelets.³⁵ Interestingly, such behavior is not observed for LMW inks which warrants further investigation that is outside the scope of this work. Above solid concentrations of 50 wt% for LMW inks and 40 wt% for HMW inks, yielding behavior seems to emerge independent of the graphene concentration. This demonstrates the high prevalence of chain entanglement driving the yielding behavior. Since the HMW binder will exhibit stronger entanglement with a lower polymer concentration, the boundary at low graphene-high solids region occurs at a lower solid concentration compared to the LMW inks.

3.1.2 | Composition dependence of yield-pseudoplastic behaviors

Figure 3 outlines the results of the flow sweep experiments for the yielding material compositions ($\tan(\delta) < 1$). Figure 3A,B outlines the variation of the yield stress for LMW and HMW inks, respectively. For both inks, the yield stress consistently increases with increasing solid and relative graphene concentration. Noting that the color scale in this figure is logarithmic, one could conclude that the yield stress increase with increasing solid and graphene concentration is near exponential within the range of 0–3000 Pa. A better view of this can be seen with 3D surface plots of the yield stress which are provided in Supporting information Figure S2. Particularly for the HMW inks, the yield stress appears to reach a plateau at the 3000–4000 Pa range for the high solid-high graphene region. Such a transition coincides with the 12 wt% absolute graphene isoline shown in Figure 2B, indicating that above the percolation threshold, the yield stress increases exponentially. Elaboration on the physical mechanisms driving this behavior requires the acquisition of more data points and is beyond the scope of this work.

Figure 3C,D outlines the variation the rate index (n) as a function of the ink composition. Fundamentally, a lower rate index in the 0–1 range indicates an increased shear thinning behavior, the rate index being equal to 1 represents a Newtonian liquid and it being larger than 1 indicates a shear thickening nature. The curve fitting has been performed by limiting the rate index range to 0–1, considering the consistent shear thinning nature of the inks. We observed that several compositions produced flow sweep data that could be represented with the

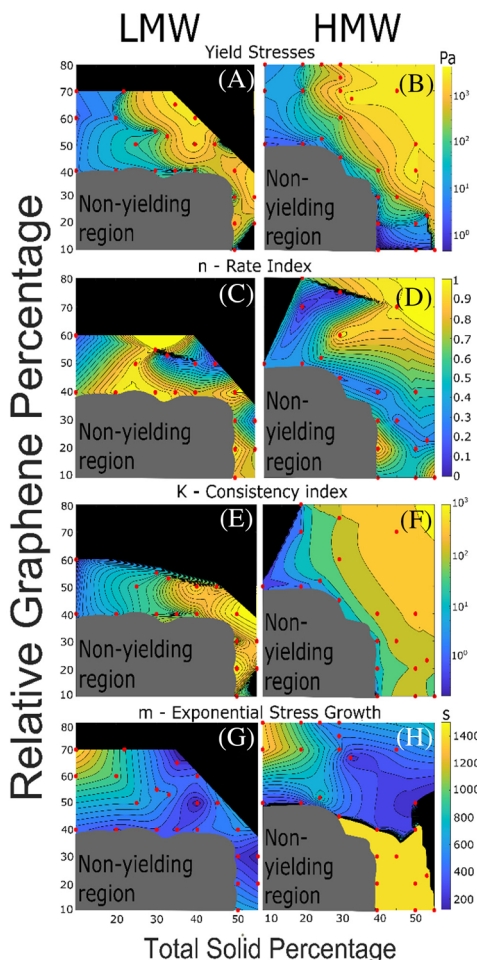


FIGURE 3 Numerical maps depicting the changes in (A, B) yield stresses, (C, D) rate indices, (E, F) consistencies, and (G, H) exponential stress growths as a function of composition. The data outside of the red points is interpolated for visualization purposes.

example given in Supporting information Figure S3. In the tested strain rate range, these compositions do not exhibit the exponential stress increase that is observed at high strain rates represented by the power-law portion of the HBP model. As such, values of K and n that are determined through the regression are mathematical rather than physical manifestations. To objectively distinguish between these compositions and the rest where the exponential increase is observed, we adopted an information criterion-based approach, similar to that presented in Section 2.3.2, to identify which version of the model best fits a given composition. Details of this approach are provided in Supporting information Figure S3. Examining the compositions that are deemed to conform to the complete HBP model, two trends emerge for both LMW and HMW binder cases: the rate index decreases with increasing graphene concentration at low solid loading (between 10 and 30 wt% solids for both LMW and HMW inks) and increasing solid concentration at low graphene loading

(i.e., increasing binder concentration). For LMW only, we can observe that the increase of both graphene and binder also leads to the reduction in the rate index, whereas the power-law portion of the high graphene-high binder region could not be observed for the HMW, limiting our ability reach a similar conclusion. These findings are expected, since the source of the shear thinning behavior is the strain rate induced microstructural alignment of ink constituents.⁹ In the low solid, high graphene region, it is anticipated that the shear thinning is primarily induced by the alignment of graphene platelets under high strain rates thus increasing graphene concentration further promotes the shear thinning effect. Similarly, in the high binder, low graphene region, the shear thinning is primarily induced by the stretching and alignment of the polymer chains, thus increasing binder concentration leads to the increased shear thinning effect. Figure 3E,F outlines the variation of the consistency (K) parameter with composition for both ink types. This parameter provides a general measure of ink viscosity. A similar behavior indicating higher viscosity (higher K) with increasing a solid concentration could be observed for both inks.

Figure 3G,H shows the variation of the m variable as a function of ink composition. This variable captures the growth of stress starting at very low strain rates and leading up to the yield stress plateau. We observed that this low strain rate behavior is a product of the temporal stress data collected at those strain rate points not reaching a steady state within the maximum data collection period of 600 s. This is demonstrated in Supporting information Figure S4. As such, a low value indicates a slower transient behavior for a given composition. As the HBP model approaches the conventional Herschel Bulkley (HB) model, where this stress growth is not observed, the m value approaches infinity. Mechanistically, considering the fact that at each data point of a flow sweep experiment, the strain is increased at a fixed rate while stress grows, a slow transient response leading up to the yield stress highlights a prominent elastic behavior, with low equivalent elastic modulus.

When the maps are examined, interestingly, the maximum values of m are observed at low solid-high graphene and high solid, low graphene regions. As such, in these compositional ranges, where one particular constituent dominates the composition over the other, the inks temporally settle faster at low strain rates and thus exhibit lower levels of elasticity. This finding indicates the presence of two competing effects. For the high graphene, low solid range, it is known that presence of graphene networks is the source of a solid-like elastic behavior and subsequent yielding (i.e., the house of cards effect). As the amount of binder chains among the

graphene platelets increase, the elasticity of the entire microstructural construct increases leading to slower transient response. Interestingly, there was significantly less transient behavior observed in binder-dominated compositions for HMW inks when compared to LMW inks. In these low graphene, high solids regions, the ink mostly consists of disassociated polymer chains that can easily yield and flow without exhibiting an elastic response. As seen in Figure 2, the threshold for binder-driven yielding is at a lower total solid concentration for HMW than LMW. The longer chains present in HMW inks leads to quicker yielding and flow, and therefore, faster transient responses at these binder-dominated compositions. This is likely behind the near HB type behavior with fast transient response for the HMW case in the high solids-low graphene region. It has been shown that these chains can bond with graphene.³⁶ One can accordingly postulate that graphene platelets act like anchors for the polymer chains at their bonding sites. As the graphene concentration increases and the platelets start inhibiting each other's motion, the chains will stretch under deformation, leading to bulk elasticity.

3.1.3 | Composition dependence of non-yielding behaviors

Figure 4 outlines the results of least squares regression fitting on flow sweeps for Carreau-Yasuda inks. Specifically, it illustrates the change in zero-shear viscosity as a function of composition. The higher-strain-rate features of the CY model, namely the consistency (λ), the rate index (n), the transition index (a), and the infinite-rate viscosity (η_∞), could not be fully captured at the lower strain rate range used in the characterization. Thus, these features will not be fully representative of true ink behavior under the conditions used and were not mapped in the same fashion as the zero-shear viscosity.

For both LMW and HMW inks, the zero-shear viscosity increases with increasing relative graphene and total solid concentrations. This is an intuitive result as the solid content increases, the interactions between the solid constituents will further prohibit flow thus leading to viscosity increase, particularly at low strain rates where shear thinning effects are not present. While the trends are the same, HMW inks appear to have an overall higher zero-shear viscosity when compared to LMW. This is likely caused by the increased entanglement between the longer chains in HMW inks.

Some non-yielding inks were best fit to the power law fluid model, and they are indicated in Supporting information Figure S5(a,b). These inks did not have a viscosity plateau within the observed strain rate range, making the

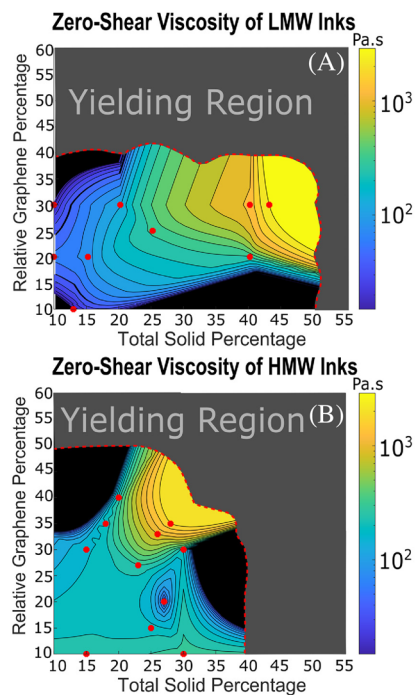


FIGURE 4 Numerical maps depicting the changes in zero-shear viscosity as a function of composition for (A) HMW and (B) LMW inks. The data outside of the red points is interpolated for visualization purposes.

zero-shear viscosity a mathematical construct rather than a physical manifestation, similar to the K and n parameters discussed in Section 3.1.2. It is likely that the plateau was not captured within the used range, and if the experiment began at a smaller strain rate the plateau would have been visible. An example of such an ink and the corresponding model fits is shown in Supporting information Figure S5(c). CY and power law AICs were used to filter out these power law inks from the remaining non-yielding inks using the same procedure outlined in Section 3.1.2. Therefore, the points indicated as power law by AIC are not shown in Figure 4.²

3.1.4 | Extensional rheology

Analysis of the extensional rheometry data was performed to understand the behavior of various ink compositions following extensional flow within the context of common capillary flow and break-up models provided in Equations (4)–(7). As noted in Section 2.3.2, to account for the variant nature of the ink behavior during the experiments, a probability calculation based on AIC analysis was performed. In that, probabilities of a given composition conforming to a set group of models were calculated. This group was formed by combining all models that exhibit the lowest AIC number for at least one ink composition.

Certain compositions required the maximum gap of 12 mm during the experiment to be lowered down to 5 mm and still exhibited no change in diameter during the relaxation period. As a result, no diameter variation data could be collected. If we interpolated a straight, horizontal line to represent the unchanging diameter, the probabilistic approach outlined in Section 2.3.2 would introduce non-physical noise by assigning probabilities to the models that we know could not physically appear in those compositional ranges. This is because AIC scores are assigned to all fitted models, and the probability calculation will assign probabilities any model with an AIC score, regardless of how poor that score is. Thus, to eliminate the risk of introducing noise into the data pool, these compositions were considered to have a 100% chance of yield stress behavior, with a 0% chance of all other models.

3.1.5 | Probability of material classifications as a function of composition

Figure 5 outlines behavior probabilities for the pooled models. Namely, these are yielding (A, B), elastic modes 1–3 (C, D), power law (E, F), and Bingham plastic (G, H). As seen in Figure 5A,B, for both binder-types, yielding compositions appear in the high graphene-high solids and high graphene-low solids regions. The two binders differ particularly in inks with high elastic fluid probability: for HMW, this behavior is more likely to appear in any low graphene composition, whereas for LMW, this behavior is most likely to occur in low graphene-high solids compositions. The low graphene-low solid region in LMW is dominated by power law and Bingham plastic behaviors. This particular difference between H- and LMW inks likely stems from the fact that unlike HMW, the LMW binder chains are not long enough to elicit elasticity at these low solid concentrations, thus there is an emergence of non-elastic fluid behavior. It is worth noting that power law and Bingham plastic models differ mathematically,³ but they still represent very similar diameter change behaviors, leading to both models exhibiting similar probabilities in the low solid-high graphene region. The Bingham plastic model captures yielding-type behavior under the assumption that the critical radius to failure is reached, shown in Equation (12). When the critical radius is achieved, filament diameter reduces abruptly, leading to failure, similar to power law.

$$R < R_c = \frac{\sigma}{\sqrt{3}\tau_y}. \quad (12)$$

The yielding-non-yielding interfaces for both HMW and LMW are indicated on the probability plots by a dashed red line. When comparing the compositional

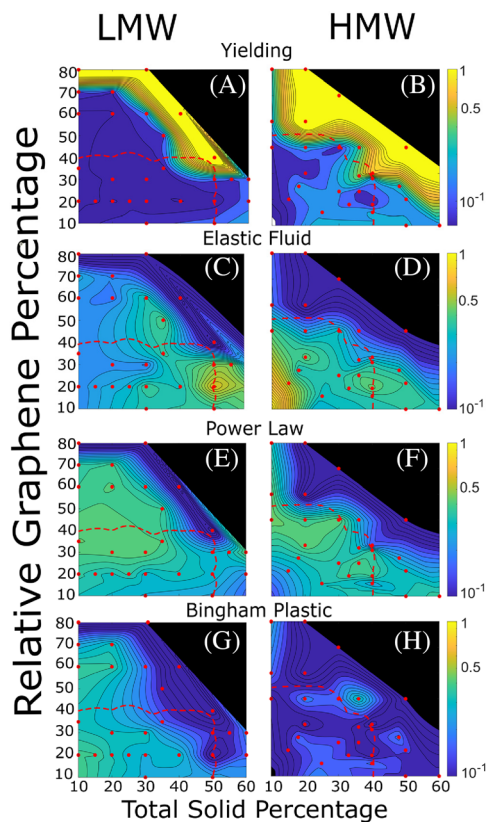


FIGURE 5 Numerical maps depicting the probability of appearance for (A, B) yielding behavior, (C, D) elastic fluid behavior, (E, F) power law behavior, and (G, H) Bingham plastic behavior as a function of composition. The data outside of the pink points is interpolated for visualization purposes. All interpolated values are percentages, so the sum of (A–H) = 1.

regions exhibiting yielding behavior as deduced from the results of the shear and extensional rheometry, one could conclude that for HMW, the boundary between high-probability yielding and high-probability elastic fluidity lies approximately where the yielding-non-yielding interface is seen in Figure 2. Interestingly, the high-probability elastic fluid and high-probability yielding regions are not separated with the yielding-non-yielding interface for LMW. Compositions below approximately 20 wt% solids and between 30 and 70 rel% graphene are most likely to have Bingham plastic or power law behavior, even though part of this region (40 rel% graphene and above) display yielding behaviors under shear. As discussed previously in this section, according to the Bingham plastic model, once a critical radius to failure is reached, the filament diameter will decrease rapidly and catastrophically fail. Equation (12) shows that as the yield stress (τ_y) decreases, the critical radius to failure increases. Because LMW inks have lower yield stresses within this region, shown in Figure 3A, it can be postulated that the critical radius to failure is likely larger than the starting radius

during relaxation for LMW inks when compared to HMW, thus leading to the increased probability of Bingham plastic materials in this region specifically.

3.1.6 | Comparison of ink behavior under shear and extension

When shear and extensional rheology are considered in tandem, it is very apparent that, largely, HBP behavior in shear coincides with yielding behavior in extension, as expected. LMW inks at 60–70 rel% graphene and 10–20 wt% total solids, a region which still exhibits a yield stress, exhibit dominantly Bingham plastic behavior. Looking at Figure 3A, it is notable that the yield stresses within this compositional area are low, leading to a larger critical radius to failure. Thus, the inks with these compositions can reach such a radius and exhibit rapid thinning and filament breakup during the relaxation. This same compositional region on the HMW map does not show Bingham plastic behavior to the same degree because the longer polymer chains in the HMW binder make the yield stress slightly larger, see Figure 3B, and therefore, the critical radius shrinks. It is likely that the critical radius for HMW inks in this region cannot be reached with our experimental setup, leading to the constant diameter during relaxation.

Elastic fluidity under extension notably coincides with Carreau–Yasuda behavior under shear. This is true for HMW inks up to 40 wt% total solids, at which point the polymer content is high enough to cause a yield stress under shear forces. Under extension, 40–60 wt% solids at 10–20 rel% graphene in HMW is still dominated by elastic fluidity because the polymer binder dominates over the graphene content enough to induce an elastic fluid response. A power law response under extension is also present in the Carreau–Yasuda region for HMW inks. As the graphene and total solid contents decrease, this shifts to the elastic fluid response. For LMW, the Carreau–Yasuda region overlaps with elastic fluid, Bingham plastic, and power law in extension. The Bingham plastic region at low graphene, low solids is likely a byproduct of the fitting algorithm, as these compositions do not exhibit a yield stress under shear. However, as mentioned in Section 3.1.5, the mathematics behind Bingham plastic and power law relaxation models are very similar. They capture similar diameter change trends, with the exception that Bingham plastic encompasses yield stress behaviors, assuming that the critical radius to failure is reached, see Equation (12). Because there is no yield stress in a non-yielding material, the non-yielding region is actually dominated by power law behavior under extension. However, if there is a high enough total solid concentration,

the polymer binder can induce an elastic fluid-type response while still within the non-yielding region.

4 | CONCLUSIONS

This article studied the composition-rheology relationships for aqueous graphene-PEO inks, focusing both on shear and extensional rheology. As a result, variations of key rheological parameters were mapped out in the compositional parameter space consisting of total solid and relative graphene concentrations. This article particularly contributes to the science of polymer composite-type precursor rheology by elucidating how (i) binder structure, specifically quantified by the molecular weight, (ii) total solid loading and (iii) the binder-filler interactions influence ink rheology. The concurrent study of shear and extensional rheology in the same compositional parameter space also provides the opportunity to investigate the correlations between the ink behavior under these different stress states. Below paragraphs summarize the key observations regarding these three aspects.

We have observed that chain length variations between H- and LMW inks led to different relative graphene concentration required to induce yielding behavior. Interestingly, inks with longer polymer chains required more graphene to yield, likely due to the long chains obstructing the graphene network formation at low concentrations. We also observed that total solid concentration is a significant variable dictating the yielding behavior, particularly at low graphene concentrations. For LMW inks, relative graphene concentration drives the yielding behavior for solid concentrations lower than a transitional level, above which inks exhibit yielding regardless of their graphene content. For HMW inks, this transitional concentration is lower. Furthermore, we observe a transition between relative graphene-concentration-driven to absolute graphene-concentration-driven yielding transition at lower solid concentrations. Intuitively, increasing solid concentration generally led to an increase in yield stress, zero-shear viscosity and consistency parameters for both ink types. Observation of ink transient behavior under shear indicated that LMW inks exhibited longer transient responses compared to HMW inks in binder-dominated compositions (low graphene and high solid).

When extensional rheology of the inks is considered, variation of the binder molecular weight led to shifting of several rheological behaviors within the compositional space. Particularly, we have observed that the elastic behavior has been mostly observed in the low graphene, high solid loading region in LMW inks, whereas it is more prominently observed in the low solid, low graphene region for HMW inks. In this particular region,

LMW ink exhibited either Bingham plastic or power law type behavior instead, which is attributed to the LMW binder chains being of insufficient length to induce an elastic fluid response.

Comparing the shear and extensional behavior of these inks, we observed the behavior indicative of the presence of yield stress under both types of stresses at high solid and graphene concentrations, as expected. Non-yielding inks predominantly demonstrated elastic fluid behavior under extension. Rather non-intuitive behavior was observed near transitional compositions between yielding and non-yielding nature (as identified by shear rheology), particularly in the form of certain inks exhibiting yielding under shear but elastic fluid response under extension.

Several other practical points should be noted while assessing the results of this study. For complex inks such as the ones studied in this work, ink stability is an important consideration as agglomeration of graphene platelets could significantly alter the ink properties. To understand if this effect is significant in our case, the level of dispersion of several inks was tested using dynamic light scattering. The dispersion quality was assessed using the polydispersity index (PDI) and the mean particle size. Details of the experimental procedure and its results can be found in Supporting information Section S4. It was concluded that, because both PDI and the mean particle size were within reasonable ranges for all the inks considered, the results presented in this work were not influenced by particle dispersion. It should further be noted that ink stability may vary over time if inks need to be stored prior to characterization/processing. As noted in Section 2.1, all of the ink characterization was performed within 48 h for each composition to minimize any effects in this study. Additionally, the rigorous mixing methods implemented in the ink preparation for this study as well as interactions between the platelets and the long polymer chains could change the molecular weight of the polymer binder due to chain scission, thus the final tested molecular weight may not be the same as that which was prescribed during ink preparation. Finally, this study exemplifies processing under ambient conditions, as changes in temperature will significantly affect the rheological properties of these precursors. Studying those rheological variations based on temperature is outside the scope of this work but would be an insightful addition to the overall generalization of polymer composite-type precursors.

The results of this study have significant practical implications regarding processing of these precursors. Particularly, several compositional regions with distinctly different behavior could be classified as favorable regions for different processing methods. For example, a

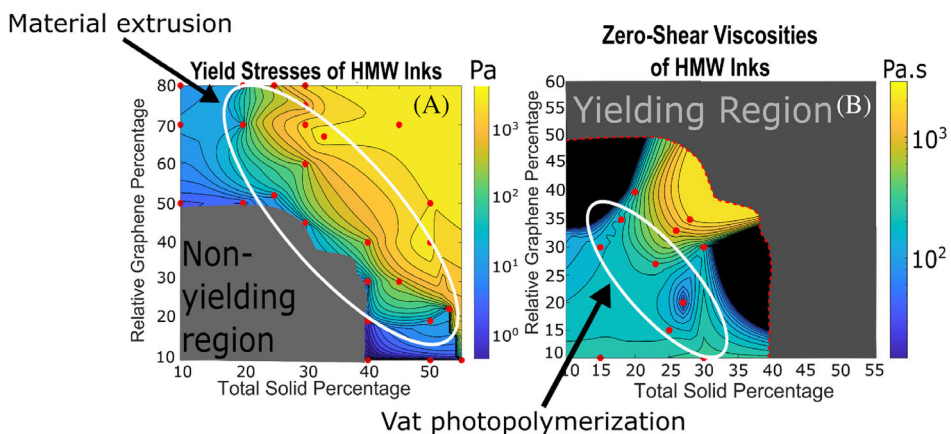


FIGURE 6 Visual descriptions of compositional regions suitable for (A) material extrusion 3D printing and (B) vat photopolymerization 3D printing, assuming the HMW rheology.

composition that exhibits a yield stress will be better suited for extrusion-based 3D printing methods, such as direct-ink-writing, because this processing method requires inks to be able to self-support their filamentary shape upon deposition, a behavior observed when inks possess the yield stress property.³⁷ On the other hand, a composition that does not exhibit yield stress will be better suited for resins in vat photopolymerization-type 3D printing. For these methods, it is essential that the resin can freely flow and coat the build plate uniformly in between the layers, which requires the lack of yield stress behavior and sufficiently low viscosities. Accordingly, if the precursors presented in this article were to be used for these applications, Figure 6 (derived from Figures 3 and 4, assuming the HMW rheology) would facilitate their compositional design. For instance, the region marked in Figure 6A would be appropriate for material extrusion since it exhibits yield stress but at a reasonably low level to not significantly increase the pressure required for extrusion. Similarly, the compositional region marked in Figure 6B would be appropriate for vat photopolymerization, given its non-yielding nature and sufficiently low viscosity. Similar practical correlations can be made for conventional manufacturing methods such as screen printing and extrusion.

Another important aspect of precursor rheology for AM is the way it affects the properties of the final part. This work can be directly applied to furthering the investigation of structural properties in additively manufactured parts, as interlayer adhesion and shape retention are both heavily influenced by rheology. The results presented here can be used to highlight compositional regions where the extrusion-based AM inks, in addition to exhibiting sufficiently high yield stress, also possess viscosities that are sufficiently low to promote chain entanglement between layers, thus increasing weld formation and mechanical performance.^{38,39} In polymer melts, polymer mobility, which is derived from

rheological measurements, plays a critical role in weld formation and directly influences part performance,⁴⁰ and is another property that can be mapped with respect to composition in a manner similar to this work.

Going forward, this research can be used as a guideline for more in-depth studies where various other compositional inputs could be considered. The results of this study are tailored for a specific material system. To apply this to other systems, the analysis should be repeated; however, this article can be applied as a roadmap to design a study for other materials as the steps of ink design, experimentation, data processing, and interpretation are all laid out in detail. Further input variables include but are not limited to filler type, solvent type, particle size, geometry, and surface chemistry, which are known to influence rheological properties.^{41–43} With data quantity and diversity increased, it would be possible to draw more generalizable conclusions and devise quantitative models describing the composition-property relationships. The specific drivers of the parameterized relationships presented in this work, such as the particular particle-binder interactions, can also be characterized and addressed in future studies. Lastly, the utilization of the data presented here can be furthered with advanced data science techniques, enabling more in-depth analysis of the experimental data and better mechanistic understanding of emergence of several behaviors. Furthermore, such techniques can enable precise prediction of material behavior within compositional ranges that were not experimentally explored, reducing the need for costly experimentation.

ACKNOWLEDGMENTS

This work has been financially supported by the National Science Foundation grant CMMI-1846758 and US Department of Defense (DoD) grant W911NF-23-2-0087.

DATA AVAILABILITY STATEMENT

The data that support the findings of this study are available from the corresponding author upon reasonable request.

ORCID

B. Arda Gozen  <https://orcid.org/0000-0002-2680-2269>

REFERENCES

- Chen J, Ding J, Shan J, et al. Recent advances in precursor-derived ceramics integrated with two-dimensional materials. *Phys Chem Chem Phys*. 2022;24(40):24677-24689. doi:[10.1039/d2cp02678c](https://doi.org/10.1039/d2cp02678c)
- Yamamura T, Ishikawa T, Shibuya M, Hisayuki T, Okamura K. Development of a new continuous Si-Ti-C-O fibre using an organometallic polymer precursor. *J Mater Sci*. 1988;23:2589-2594.
- Liu S, Qin S, He M, Zhou D, Qin Q, Wang H. Current applications of poly(lactic acid) composites in tissue engineering and drug delivery. *Compos B Eng*. 2020;199:199. doi:[10.1016/j.compositesb.2020.108238](https://doi.org/10.1016/j.compositesb.2020.108238)
- Binner J, Porter M, Baker B, et al. Selection, processing, properties and applications of ultra-high temperature ceramic matrix composites, UHTCMCs-a review. *Int Mater Rev*. 2020;65(7):389-444. doi:[10.1080/09506608.2019.1652006](https://doi.org/10.1080/09506608.2019.1652006)
- Ayode Obitoju T, Ugochukwu Okoye P, Chen G, Li Y, Onyeka Okoye M, Li S. Advanced ceramic components: materials, fabrication, and applications. *J Ind Eng Chem*. 2020;85:34-65. doi:[10.1016/j.jiec.2020.02.002](https://doi.org/10.1016/j.jiec.2020.02.002)
- Lu X, Lee Y, Yang S, Hao Y, Evans JRG, Parini CG. Solvent-based paste extrusion solid freeforming. *J Eur Ceram Soc*. 2010;30(1):1-10. doi:[10.1016/j.jeurceramsoc.2009.07.019](https://doi.org/10.1016/j.jeurceramsoc.2009.07.019)
- Rajabifar N, Rostami A. Investigation of the effect of hybrid nanofiller on the mechanical performance and surface properties of bio-based polylactic acid/polyolefin elastomer (PLA/POE) blend. *Polymers (Basel)*. 2023;15(12):2708. doi:[10.3390/polym15122708](https://doi.org/10.3390/polym15122708)
- Rajabifar N, Jalali-Arani A. A new nanocomposite based on polylactic acid/butadiene rubber/clay: morphology development and mechanical properties. *J Appl Polym Sci*. 2024;141(7):e54961. doi:[10.1002/app.54961](https://doi.org/10.1002/app.54961)
- Lewicki JP, Rodriguez JN, Zhu C, et al. 3D-printing of mesostructurally ordered carbon fiber/polymer composites with unprecedented orthotropic physical properties. *Sci Rep*. 2017;7:7. doi:[10.1038/srep43401](https://doi.org/10.1038/srep43401)
- Raney JR, Compton BG, Mueller J, Ober TJ, Shea K, Lewis JA. Rotational 3D printing of damage-tolerant composites with programmable mechanics. *Proc Natl Acad Sci U S A*. 2018;115(6):1198-1203. doi:[10.1073/pnas.1715157115](https://doi.org/10.1073/pnas.1715157115)
- Niu H, Guo H, Kang L, Ren L, Lv R, Bai S. Vertical alignment of anisotropic fillers assisted by expansion flow in polymer composites. *Nanomicro Lett*. 2022;14(1):153. doi:[10.1007/s40820-022-00909-2](https://doi.org/10.1007/s40820-022-00909-2)
- Markandan K, Lai CQ. Fabrication, properties and applications of polymer composites additively manufactured with filler alignment control: a review. *Compos B Eng*. 2023;256:256. doi:[10.1016/j.compositesb.2023.110661](https://doi.org/10.1016/j.compositesb.2023.110661)
- Cassagnau P. Melt rheology of organoclay and fumed silica nanocomposites. *Polymer (Guildf)*. 2008;49(9):2183-2196. doi:[10.1016/j.polymer.2007.12.035](https://doi.org/10.1016/j.polymer.2007.12.035)
- Hyun YH, Lim ST, Choi HJ, John MS. Rheology of poly(ethylene oxide)/organoclay nanocomposites. *Macromolecules*. 2001;34(23):8084-8093. doi:[10.1021/ma002191w](https://doi.org/10.1021/ma002191w)
- Gelfer MY, Song HH, Liu L, et al. Effects of organoclays on morphology and thermal and rheological properties of polystyrene and poly(methyl methacrylate) blends. *J Polym Sci B*. 2002;41(1):44-54. doi:[10.1002/polb.10360](https://doi.org/10.1002/polb.10360)
- Walls HJ, Zhou J, Yerian JA, et al. Fumed silica-based composite polymer electrolytes: synthesis, rheology, and electrochemistry. *J Power Sources*. 2000;89:156-162. www.elsevier.com/locate/jpowsour
- Arrigo R, Malucelli G. Rheological behavior of polymer/carbon nanotube composites: an overview. *Materials*. 2020;13(12):1-27. doi:[10.3390/ma13122771](https://doi.org/10.3390/ma13122771)
- Ren D, Zheng S, Wu F, Yang W, Liu Z, Yang M. Formation and evolution of the carbon black network in polyethylene/carbon black composites: rheology and conductivity properties. *J Appl Polym Sci*. 2014;131(7):39953. doi:[10.1002/app.39953](https://doi.org/10.1002/app.39953)
- Sahu SK, Badgayan ND, Sreekanth PSR. Rheological properties of hdpe based thermoplastic polymeric nanocomposite reinforced with multidimensional carbon-based nanofillers. *Biointerface Res Appl Chem*. 2022;12(4):5709-5715. doi:[10.33263/BRIAC124.57095715](https://doi.org/10.33263/BRIAC124.57095715)
- Thomas S, Muller R, Abraham J. *Rheology and Processing of Polymer Nanocomposites*. John Wiley & Sons, Inc; 2016.
- Payne AR. The dynamic properties of carbon black loaded natural rubber vulcanizates. Part II. *J Appl Polym Sci*. 1962;36:472:57-63.
- Ansari S, Giannelis EP. Functionalized graphene sheet-poly(vinylidene fluoride) conductive nanocomposites. *J Polym Sci B*. 2009;47(9):888-897. doi:[10.1002/polb.21695](https://doi.org/10.1002/polb.21695)
- Ramanathan T, Abdala AA, Stankovich S, et al. Functionalized graphene sheets for polymer nanocomposites. *Nat Nanotechnol*. 2008;3(6):327-331. doi:[10.1038/nnano.2008.96](https://doi.org/10.1038/nnano.2008.96)
- Anderson BJ, Zukoski CF. Rheology and microstructure of entangled polymer nanocomposite melts. *Macromolecules*. 2009;42(21):8370-8384. doi:[10.1021/ma9011158](https://doi.org/10.1021/ma9011158)
- Rueda MM, Auscher MC, Fulchiron R, et al. Rheology and applications of highly filled polymers: a review of current understanding. *Prog Polym Sci*. 2017;66:22-53. doi:[10.1016/j.progpolymsci.2016.12.007](https://doi.org/10.1016/j.progpolymsci.2016.12.007)
- Zhang Y, Zhu Y, Zheng S, et al. Ink formulation, scalable applications and challenging perspectives of screen printing for emerging printed microelectronics. *J Energy Chem*. 2021;63:498-513. doi:[10.1016/j.jechem.2021.08.011](https://doi.org/10.1016/j.jechem.2021.08.011)
- Spiegelberg SH, Ables DC, McKinley GH. The role of end-effects on measurements of extensional viscosity in filament stretching rheometers. *J Non-Newtonian Fluid Mech*. 1996;64:229-267.
- Tandel R, Gozen BA. Direct-ink-writing of liquid metal-graphene-based polymer composites: composition-processing-property relationships. *J Mater Process Technol*. 2022;302:302. doi:[10.1016/j.jmatprotec.2021.117470](https://doi.org/10.1016/j.jmatprotec.2021.117470)
- Herschel WH, Bulkley R. *Konsistenzmessungen von Gummi-Benzollösungen*. Vol 39. Springer Nature; 1926:291-300.

30. Papanastasiou TC. Flows of materials with yield. *J Rheol (N Y N Y)*. 1987;31(5):385-404. doi:[10.1122/1.549926](https://doi.org/10.1122/1.549926)
31. Yasuda K, Armstrong RC, Cohen RE. Shear flow properties of concentrated solutions of linear and star branched polystyrenes. *Rheol Acta*. 1981;20:163-178.
32. McKinley GH. *Visco-elasto-capillary thinning and break-up of complex fluids*. 2005 <http://web.mit.edu/fluids>
33. Akaike H. *Information theory and an extension of the maximum likelihood principle*. 1972.
34. Hartnett JP, Hu RYZ. Technical note: the yield stress—an engineering reality. *J Rheol (N Y N Y)*. 1989;33(4):671-679. doi:[10.1122/1.550006](https://doi.org/10.1122/1.550006)
35. Zotti A, Zuppolini S, Borriello A, Zarrelli M. Polymer nanocomposites based on graphite nanoplatelets and amphiphilic graphene platelets. *Compos B Eng*. 2022;246:246. doi:[10.1016/j.compositesb.2022.110223](https://doi.org/10.1016/j.compositesb.2022.110223)
36. Gudarzi MM, Sharif F. Molecular level dispersion of graphene in polymer matrices using colloidal polymer and graphene. *J Colloid Interface Sci*. 2012;366(1):44-50. doi:[10.1016/j.jcis.2011.09.086](https://doi.org/10.1016/j.jcis.2011.09.086)
37. Lewis JA, Smay JE, Stuecker J, Cesarano J. Direct ink writing of three-dimensional ceramic structures. *J Am Ceram Soc*. 2006;89(12):3599-3609. doi:[10.1111/j.1551-2916.2006.01382.x](https://doi.org/10.1111/j.1551-2916.2006.01382.x)
38. Das A, Gilmer EL, Biria S, Bortner MJ. Importance of polymer rheology on material extrusion additive manufacturing: correlating process physics to print properties. *ACS Appl Polym Mater*. 2021;3(3):1218-1249. doi:[10.1021/acsapm.0c01228](https://doi.org/10.1021/acsapm.0c01228)
39. Gao X, Qi S, Kuang X, Su Y, Li J, Wang D. Fused filament fabrication of polymer materials: a review of interlayer bond. *Addit Manuf*. 2021;37:37. doi:[10.1016/j.addma.2020.101658](https://doi.org/10.1016/j.addma.2020.101658)
40. Seppala JE, Hoon Han S, Hillgartner KE, Davis CS, Migler KB. Weld formation during material extrusion additive manufacturing. *Soft Matter*. 2017;13(38):6761-6769. doi:[10.1039/c7sm00950j](https://doi.org/10.1039/c7sm00950j)
41. Lee JH, Um CM, Lee I. Rheological properties of resin composites according to variations in monomer and filler composition. *Dent Mater*. 2006;22(6):515-526. doi:[10.1016/j.dental.2005.05.008](https://doi.org/10.1016/j.dental.2005.05.008)
42. Sutar H, Mishra B, Senapati P, Murmu R, Sahu D. Mechanical, thermal, and morphological properties of graphene nanoplatelet-reinforced polypropylene nanocomposites: effects of nanofiller thickness. *J Compos Sci*. 2021;5(1):24. doi:[10.3390/jcs5010024](https://doi.org/10.3390/jcs5010024)
43. Chen J, Li L. Effect of oxidation degree on the thermal properties of graphene oxide. *J Mater Res Technol*. 2020;9(6):13740-13748. doi:[10.1016/j.jmrt.2020.09.092](https://doi.org/10.1016/j.jmrt.2020.09.092)

SUPPORTING INFORMATION

Additional supporting information can be found online in the Supporting Information section at the end of this article.

How to cite this article: Grover CA, Bernal CB, Sargin I, Beckman SP, Gozen BA. Mapping of composition-rheology relationships in polymer composite-type precursors. *Polym Compos*. 2025; 46(5):4021-4034. doi:[10.1002/pc.29220](https://doi.org/10.1002/pc.29220)